Time-gated viewing studies on tissuelike phantoms

Berg, R; Andersson-Engels, Stefan; Jarlman, O; Svanberg, Sune

Published in:
Applied Optics

DOI:
10.1364/AO.35.003432

1996

Time-gated viewing studies on tissuelike phantoms

R. Berg, S. Andersson-Engels, O. Jarlman, and S. Svanberg

A time-gated technique to enhance viewing through highly scattering media such as tissue is discussed. Experiments have been performed on tissuelike plastic phantoms to determine the possibilities and limitations of the technique. The effects of the time-gate width and the localization, size, and optical properties of hidden objects have been studied. A computer model to simulate light propagation in tissue is also presented. The predictions of the model are compared with experimental results.

Key words: Medical diagnostics, time-gated viewing, tissue optics, transillumination, scattering media, diffusion equation, numerical modeling.

1. Introduction

The challenge of looking through highly scattering materials such as tissue by the use of low-energy photons is a growing field of interest.[1] The task has been promoted by a desire to develop a method to perform screening for breast cancer with safe doses of optical radiation instead of potentially harmful ionizing x rays.[2,3] The wavelength region of interest is approximately 650–1300 nm, where transmission through tissue is highest.[4] The dilemma encountered when breast imaging is performed at these wavelengths is that the dominating attenuation process is scattering. This leads to blurred images and poor resolution. Typical values for the scattering coefficient μ_s of tissue in this wavelength region are in the range of 5–50 mm^{-1}. This range implies that the main number of photons that have traveled through a few centimeters of tissue have been scattered several thousand times.

Several new techniques to improve optical tissue-transillumination imaging are under development.[1,5,6] The new modalities can be divided into two major groups: time- and frequency-domain methods. The time-domain methods are based on irradiating the tissue with ultrashort laser pulses and on using time-resolved detection of the transmitted light. An enhanced image of objects located deeply inside the tissue can be accomplished by the use of the very first arriving photons only. They have traveled the straightest and shortest path through the tissue and thus give a higher spatial resolution. Different methods of performing time-resolved detection have been used. One technique is based on holographic detection, in which the first transmitted photons are gated out by the use of the coherent interference between this light and a gate pulse on a holographic plate.[7,8] This technique implies, as a result of the demand of coherence, that the first light exiting the tissue is coherent with the laser pulse. Light delayed because of multiple scattering in the tissue has lost the coherence and thus contributes to an undesirable background. This background makes this technique not useful in practice for transilluminating tissues of some centimeters in thickness. The imaging technique developed by Inaba *et al.*[9] is also dependent on the coherence of the transmitted light. Other techniques are based on ultrafast gating by the use of different types of nonlinear optical phenomena, such as second-harmonic generation,[10] the optical Kerr effect,[11] stimulated Raman amplification,[12] or upconversion.[13] These techniques require lasers with high peak powers to drive the nonlinear optical device. Time-resolved detection can also be attained with fast electronic devices. The streak camera gives a temporal resolution of the order of 1–10 ps, depending on the operational mode, and it has been used by some groups for tissue $\zeta\psi$ transillumination studies.[14,15]

R. Berg, S. Andersson-Engels, and S. Svanberg are with the Department of Physics, Lund Institute of Technology, P.O. Box 118, S-221 00 Lund, Sweden; O. Jarlman is with the Department of Diagnostic Radiology, Lund University Hospital, S-221 85 Lund, Sweden.

Received 20 July 1995; revised manuscript received 2 January 1996.

0003-6935/96/193432-09$10.00/0

In this paper we present research performed using time-correlated single-photon counting as the detection technique.[5,16] This modality has a temporal resolution of roughly 30–100 ps and a wide dynamic range.

The frequency-domain approach for tissue transillumination is based on irradiation of the sample with intensity-modulated light and detection of the demodulation of the amplitude and the change of phase of the exiting light.[17,18] As light sources rf-modulated diode lasers and mode-locked lasers have been used. The detection is based on heterodyne or frequency-mixing actions.

The time- and frequency-domain techniques can also be used for tissue characterization.[19] By analysis of the temporal dispersion of the transmitted or backscattered light, the optical properties of the tissue can be determined. These properties are interesting, e.g., for photodynamic therapy or tissue diagnostics. Tissue oxygenation can also be determined with these techniques.[20,21]

Conventional transillumination breast imaging (diaphanography) is based on the detection of tumors because of their elevated absorption, which is caused by the increased blood supply that many tumors have. However, we have shown that the time-gated, as well as the frequency-domain, technique is much more sensitive to the scattering coefficient than to the absorption coefficient.[22] In this paper we show the ability of our system to detect tumor phantoms, depending on their size and localization in the tissue phantom. The effects of the optical properties of the hidden object are also studied experimentally, and we verify our experimental data using a numerical model developed at our department.[23] The model is also used to expand the study of the optical properties beyond the experimental data.

2. Materials and Methods

A. Experimental Setup

The experimental arrangement used for time-resolved transillumination is illustrated in Fig. 1. The light source was a mode-locked argon-ion laser pumping a dye laser. The pulse length from the dye laser was measured with an autocorrelator to be 6 ps. The dye laser was equipped with a cavity dumper (and its driver), making it possible to alter the repetition rate from the laser. In all the experiments reported in this paper the repetition rate was 10 MHz and the wavelength 670 nm. The average power was approximately 50 mW. The laser light irradiated the sample, and the transmitted light was collected on the opposite side by a clear-cut 600-μm-diameter optical fiber. The light exiting the fiber was focused onto the detector through an interference filter to reduce the influence of ambient light. The time-correlated single-photon counting detection technique was employed. A fast detector (Hamamatsu, Model R1564U-07 MCP-PMT) was

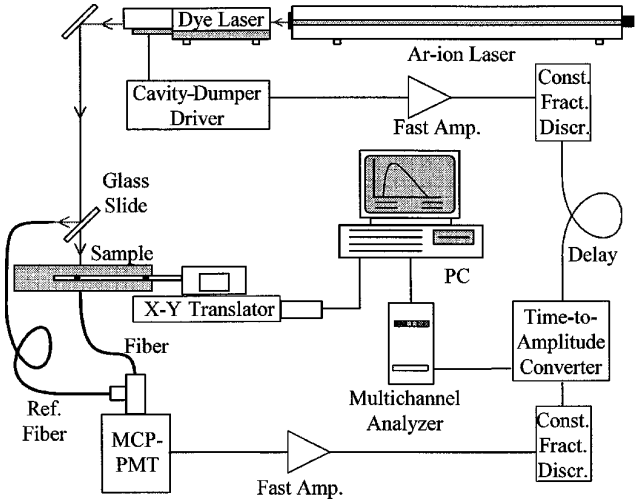

Fig. 1. Diagram of experimental setup used in the time-gated viewing experiments. Const. Fract. Discr., constant fraction discriminator; Ref., reference; Amp., amplifier.

used. The signal for each detected photon was amplified with a fast amplifier, fed through a constant fraction discriminator, and worked as a start signal for the time-to-amplitude converter. The stop signal was taken from the cavity-dumper driver unit through an amplifier and a constant-fraction discriminator, to the time-to-amplitude converter. The output voltage from the time-to-amplitude converter was fed to a multichannel analyzer, in which the temporal histograms were assembled. The temporal-response function for the system was approximately 70 ps (FWHM). To compensate for any drift phenomena in the system, a small part of the incident light was reflected off by a glass slide and directed to the detector through an optical fiber, providing a reference peak in time. The reference peak is located in time when it does not interfere with the light exiting the sample. The curves were read out to a PC for on-line evaluation. The computer also controlled the scanning over the sample by means of stepping motors.

B. Tissue Phantom

The tissue phantom in all experiments consisted of a white, highly scattering plastic called Delrin (DuPont). We estimated the optical properties of the plastic by fitting an experimental time-dispersion curve of light transmitted through a homogeneous slab with the solution to the diffusion equation presented by Patterson *et al.*[24] Figure 2 shows the temporal-dispersion curve obtained when a 30-mm-thick slab of Delrin was transilluminated (filled-squares curve). The figure also shows the fit to the analytical model (solid curve), from which the optical properties were extracted. The optical properties were $\mu_s' = 2.3\ \mathrm{mm}^{-1}$ and $\mu_a = 0.002\ \mathrm{mm}^{-1}$ [μ_s' is the effective scattering coefficient, i.e., $(1 - g) \times \mu_s$, where g is the scattering anisotropy coefficient (the average of the cosine of the scattering angle), μ_a is

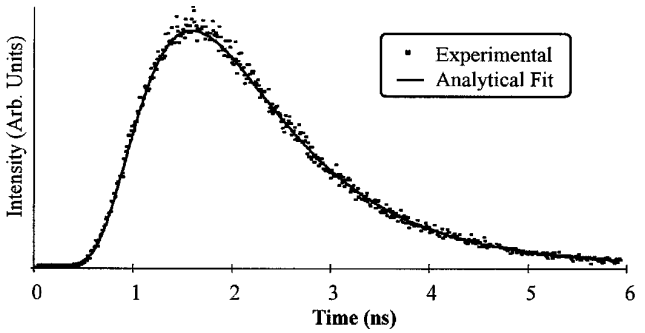

Fig. 2. Temporal-dispersion data: The filled squares form a typical experimental time-dispersion curve, obtained when 30 mm of Delrin plastic were transilluminated. The solid curve is a fit to the analytical solution of the diffusion equation, giving the optical properties of the plastic ($\mu_s' = 2.3\ \text{mm}^{-1}$ and $\mu_a = 0.002\ \text{mm}^{-1}$).

the absorption coefficient]. The plastic is thus a highly scattering medium with low absorption. We used 5-mm-thick slabs of the plastic. Holes of different sizes were drilled into the plastic to act as tumor phantoms. The holes were either empty or filled with liquid to simulate different optical properties of the tumor. Stacking the slabs of plastic yielded different thicknesses for the model and positions of the tumor. Silicon oil with the same refractive index as the plastic was used between the plastic slabs to reduce the effect of any air pockets.

C. Computer Model

Two frequently used techniques for modeling near-infrared light fluence in tissue are Monte Carlo simulations[25] and analytical or numerical solutions of the diffusion approximation to the Boltzmann transport equation.[26,27] The basis for the Monte Carlo technique is tracing a large number of photon paths that traverse the tissue from the photon source through a multiple-scattering medium to the photon detector. The scattering events within the tissue are determined by a probability function that matches the scattering coefficient. At each scattering event a part of the ray, determined by the absorption coefficient, is absorbed. The scattering angle is given by the scattering phase function. A Monte Carlo algorithm can simulate the photon flux accurately for a wide range of geometries and optical parameters of the tissue slab. Monte Carlo simulations, however, require a high computer capacity to obtain statistically good, quality data. The diffusion equation can be derived from the transport equation if the coherent radiance is neglected and the diffuse radiance is assumed to be only linearly dependent on the direction of the photon velocity. With this approximation, and the further assumption that the rate of change in the photon flux is much smaller than the reduced collision rate multiplied by the photon flux, the Boltzmann transport equation can be simplified to yield the diffusion equation:

$$\frac{n}{c}\frac{\partial\phi(\mathbf{r}, t)}{\partial t} - \nabla[D\nabla\phi(\mathbf{r}, t)] + \mu_a\phi(\mathbf{r}, t) = S(\mathbf{r}, t), \quad (1)$$

where $\phi(\mathbf{r}, t)$ is the diffuse photon fluence rate, c is the speed of light in vacuum, n is the refractive index of the tissue, D is the diffusion coefficient, i.e., $D = [3(\mu_a + (1 - g)\mu_s)]^{-1}$, and $S(\mathbf{r}, t)$ is the photon source. In Eq. (1) the tissue is characterized with an absorption and a scattering coefficient (μ_a and μ_s, respectively) and the mean cosine of the scattering function (g). This approximation is valid if $\mu_s(1 - g) \gg \mu_a$ for the photon fluence rate at a distance from the source and some time after an impulse source injection. We are interested in the light fluence rate far from the source but within a relatively short time window following the irradiation pulse. In this situation the diffusion approximation may not be accurate. However, here we are interested in qualitative rather than quantitative behavior, and thus this approximation should be acceptable for the study of the relative sensitivity of the fluence rate to variations in absorption and scattering coefficients inside a turbid medium.

This equation can be solved analytically in certain simple geometries. For our studies, we chose to use a numerical solution of the diffusion approximation. This model allows us to vary freely both the scattering and the absorption coefficient within the slab and to compare weak signals without problems with photon statistics. The diffusion equation was translated to a difference equation for finite steps of the x, y, z, and t variables, and a generalized Crank–Nicholson algorithm for three dimensions, the alternating-direction implicit method, was employed.[28] This method solves each spatial dimension separately using a third of a time step for the x, y, and z dimensions, respectively. The resulting equation for the x dimension is

$$\begin{aligned}\phi_{xyz}^{t+1/3} - \phi_{xyz}^{t} = \frac{c\Delta t}{3n\Delta^2}\Big[&D_{x+1/2yz}\left(\phi_{x+1yz}^{t+1/3} - \phi_{xyz}^{t+1/3}\right)\\ &- D_{x-1/2yz}\left(\phi_{xyz}^{t+1/3} - \phi_{x-1yz}^{t+1/3}\right)\\ &+ D_{xy+1/2z}\left(\phi_{xy+1z}^{t} - \phi_{xyz}^{t}\right)\\ &- D_{xy-1/2z}\left(\phi_{xyz}^{t} - \phi_{xy-1z}^{t}\right)\\ &+ D_{xyz+1/2}\left(\phi_{xyz+1}^{t} - \phi_{xyz}^{t}\right)\\ &- D_{xyz-1/2}\left(\phi_{xyz}^{t} - \phi_{xyz-1}^{t}\right)\Big]\\ &- \frac{c\Delta t}{6n}\mu_a\left(\phi_{xyz}^{t} + \phi_{xyz}^{t+1/3}\right), \end{aligned} \quad (2)$$

where ϕ_{xyz}^{t} is the fluence rate in the matrix element (x, y, z) at time t, Δt is the time step, Δ is the step size in x, y, and z, and $D_{x+1/2yz}$ is the average of the diffusion coefficient in the matrix elements (x, y, z) and $(x + 1, y, z)$. Similar equations are obtained for

the y and z dimensions. To solve for the x dimension requires that a tridiagonal system of equations be solved for every y and z coordinate.

3. Results

A. Gate Width

To measure the effects of the time-gate width we used a 30-mm-thick slab of Delrin with a 5-mm-diameter hole. The hole was located in the middle of the slab and was empty. We performed a scan transversally to the direction of the hole with 1 mm between every measuring point. The total scan length was 30 mm. The lower part of Fig. 3 shows the measurement geometry. The recording time was 10 s/point. The upper part of Fig. 3 shows a plot of the light intensity in a 230-ps-long gate divided by the total amount of light detected. This time gate corresponds to a light intensity of 0.1% of the total light for regions far from the hole. This division is done to minimize the influence of some artifacts, such as intensity variations in the laser and dirt on the sample surfaces. As can be seen there is more early light detected in the region of the hole than beside it. This effect has been shown in previous studies and is due to the low scattering coefficient in the hole.[22] To quantify this effect in the scan obtained, we fitted it to a Gaussian curve.

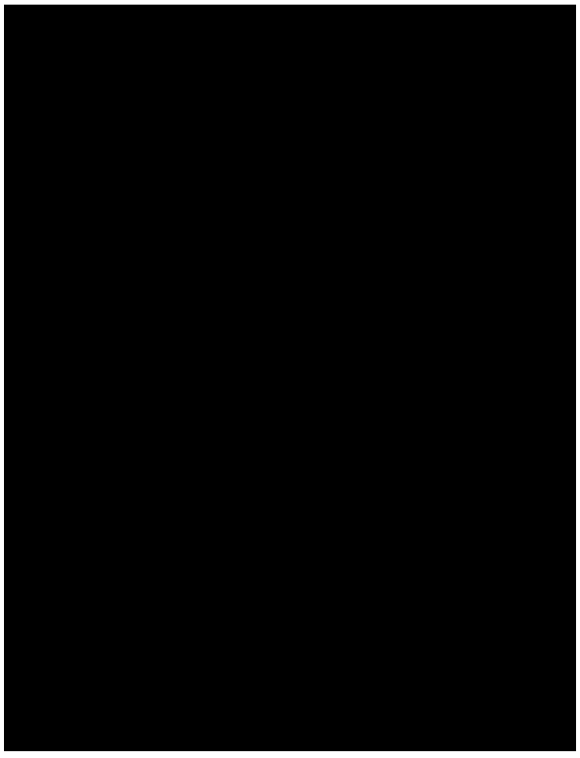

Fig. 3. Diagram of the geometry used during transillumination of the tissue phantoms (lower image). The curve (upper plot) shows the relative amount of light detected in the time-gate window used. The letters A, B, and C represent the detected relative light intensity within the time gate and the change of the light intensity that is due to the hidden object when the phantom is scanned.

It turns out that the scan obtained fits a Gaussian curve quite well. The letters in the figure denote certain features of the curve: A is the relative amount of light obtained in regions far from the empty hole; B is the relative amount of light in the empty-hole region; and C is the FWHM of the peak in the obtained scan. In Fig. 4 it is shown how these parameters change when the time-gate width is changed. Figure 4(a) shows the relative amount of light obtained at different gate widths (A). The gate starts when the signal starts to rise. Figure 4(b) shows the relative contrast, i.e., B/A. As can be seen, the shorter the time gate, the higher the contrast. Figure 4(c) shows the FWHM (C) of the scan, and Fig. 4(d) shows the residual from the least-squares fit of the Gaussian curve and the scan, i.e., this curve shows the noise. As can be seen the noise is low down to an ~250-ps time-gate width, at which point the noise starts to rise. When we evaluated the experimental curves discussed in the following sections, we chose a time-gate window that starts at the value of the signal as it begins to rise up to where the noise [Fig. 4(d)] has become low. We chose a time gate of 230 ps, which also corresponds to that 0.1% of the total light reading the detector that falls into this gate if measured at a position far from the empty hole.

B. Effects of Hole Size

A series of scans with different hole sizes was performed to determine the spatial resolution of the system. The geometry and size of the phantom was exactly as described in Section 3.A. The diameter of the empty hole in the middle of the slab was altered between 8 and 3 mm. Figure 5 shows the relative contrast B/A and the FWHM C of the different scans. As the plot shows, the hole can be seen down to a size of ~4 mm. The curves comprise an average of five scans and include error bars. Clearly the contrast is highly dependent of the size of the hole, but the FWHM is not.

C. Effects of Hole Position

We also wanted to study the influence of the position of the hole in the phantom. Figure 6 shows the relative contrast B/A and the FWHM C as functions of the hole position. As Fig. 6 illustrates, the hole is most difficult to detect when it is located in the middle of the phantom.

D. Numerical Modeling

The numerical computer model was compared with experimental results to verify the model. For the numerical solutions calculated in this study a ($x = 31$, $y = 31$, $z = 20$) matrix was used. This size of the matrix is sufficient to give a reliable result.[29] To obtain a time-dispersion curve, which is approximately 6 ns long, we required a computer time of 10 min on a 150-MHz Digital Equipment Company Alpha PC. Experimental scans were performed over a 30-mm-thick slab of Delrin with a 5-mm-diameter hole in the middle. The hole was filled with a mix of

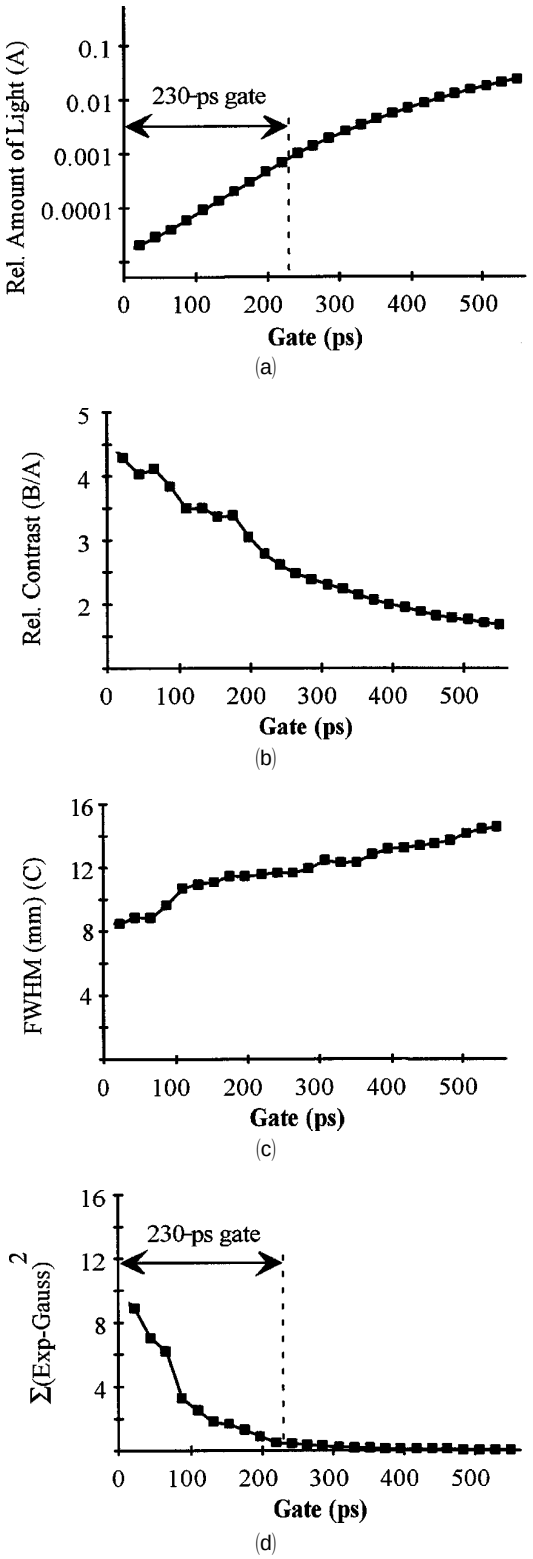

Fig. 4. Plots of the influence of the time-gate width when a 30-mm-thick tissue phantom ($\mu_s' = 2.3$ mm^{-1} and $\mu_a = 0.002$ mm^{-1}) containing a 5-mm hole in the middle is transilluminated: (a) The relative (Rel.) amount of light A detected as a function of the width of the gate window. (b) The contrast (B/A) in the detection of the hidden object. (c) The FWHM C in the detection of the hidden object. (d) The residual between the experimental curve and the Gaussian fit. The 230-ps gate used during evaluation of the experimental curves is also indicated in (a) and (d).

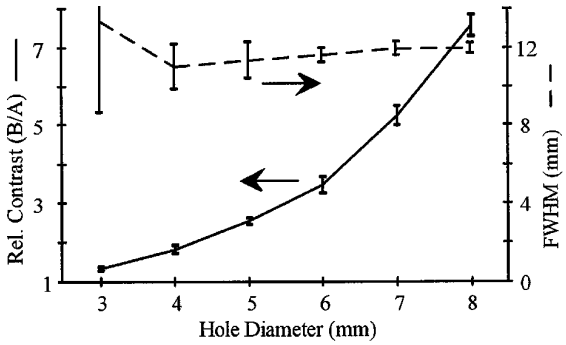

Fig. 5. Experimental curves obtained from the transillumination of a 30-mm-thick tissue phantom ($\mu_s' = 2.3$ mm^{-1} and $\mu_a = 0.002$ mm^{-1}) containing holes of varying sizes located in the middle of the phantom. The diagram shows the relative contrast B/A (solid curve) and the FWHM C (dashed curve) as functions of the hole size.

Intralipid (Kabi Pharmacia) as a scatterer and a laser dye (Rh 700, Lambda Physik) as an absorber. To avoid an influence from fluorescence in the dye, a filter that transmitted only the laser wavelength was placed in front of the detector. The optical properties of the two constituents were estimated separately with a simple narrow-beam experiment on diluted samples of each constituent. The scattering coefficient of Intralipid was estimated to 601 ± 85 mm^{-1} for 1 g/ml pure Intralipid. The g factor was taken from the literature to be 0.7.[30] The laser dye was mixed to a stock solution with an absorption coefficient of $\mu_a = 1.47$ mm^{-1}, which was then diluted to the appropriate concentration. Figure 7 shows a typical scan in which the optical properties of the mixture were estimated to be $\mu_s' = 0.56$ mm^{-1} and $\mu_a = 0.029$ mm^{-1}, i.e., the cylinder-shaped hole had lower scattering and higher absorption than the surrounding Delrin ($\mu_s' = 2.3$ mm^{-1}, $\mu_a = 0.002$ mm^{-1}). The numerical model was used to simulate the same type of scan. The solid curves with squares in Figs. 7 show the experimental results and the dashed curves with triangles the results obtained with the numerical model. The curves in Fig. 7(a) show the first 230 ps of light, and those in Fig. 7(b)

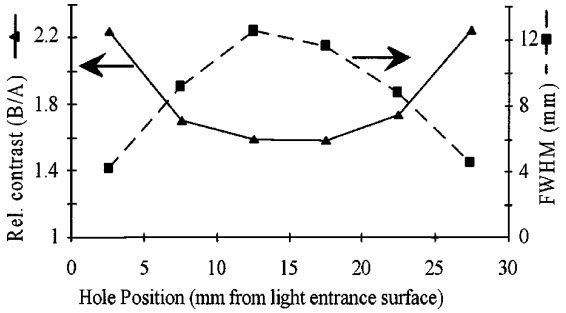

Fig. 6. Experimental curves obtained by transillumination of a 30-mm-thick tissue phantom ($\mu_s' = 2.3$ mm^{-1}, $\mu_a = 0.002$ mm^{-1}) containing a 4-mm hole at different distances from the surface at which the light enters the phantom. The diagram shows the relative contrast B/A (triangles) and the FWHM C (squares) as functions of the hole position.

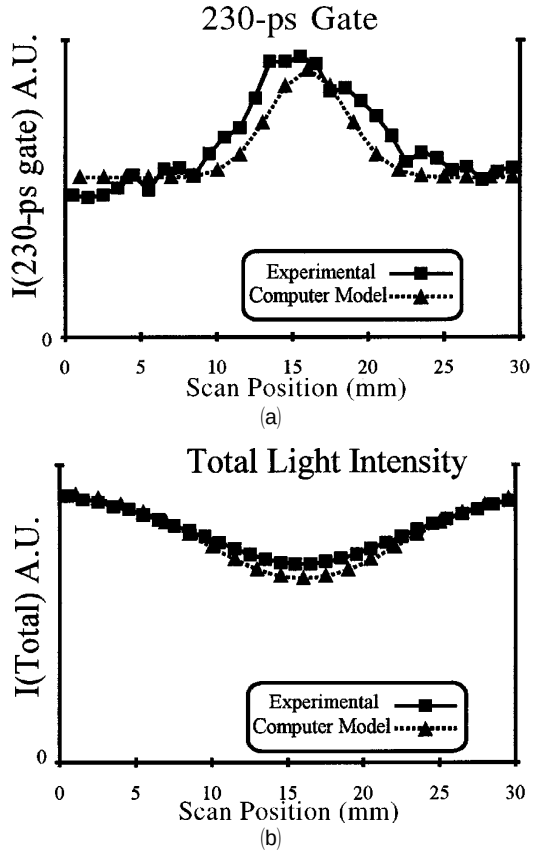

Fig. 7. Comparison between the experimental results and the numerical computer model of the transillumination of a 30-mm-thick tissue phantom containing a 5-mm hole filled with a liquid that has a lower scattering coefficient and a higher absorption coefficient than the phantom: (a) the first light detected in a 230-ps time gate, and (b) the total light intensity obtained as a function of the scan position.

show the total light intensity obtained at each measurement point. As can be seen the amount of total light decreases when the scan passes over the cylinder because of the increased absorption, whereas the time-gated light intensity increases because of the lower scattering in the cylinder.

Because of the rather low resolution of the numerical model, it is not possible to simulate a 5-mm cylindrical hole. It has to be simulated with a 5-voxel cross in cross section. In the Boltzmann transport equation, from which the diffusion approximation is derived, the description of the fluence flow in and out of a voxel is given by the partial derivative in space multiplied by the surface area of the voxel. This is transformed with Gauss' theorem into a volume integral:

$$\oint \nabla\phi(\mathbf{r}, t)\mathrm{d}S = \int \Delta\phi(\mathbf{r}, t)\mathrm{d}V. \qquad (3)$$

Looking more carefully at Eq. (2) we can see that also in the numerical model the flow into a voxel is proportional to the gradient of the fluence times the surface area of the voxel, whereas the absorption scales with the volume of the voxel. To describe the 5-mm hole in the model correctly, one must choose the surface area of the 5-voxel cross to be the same as that of the cylindrical holes. Thus the volume will not be correct, but this is solved when the absorption coefficient of the hole is scaled a factor corresponding to the difference in volume. In our model the difference was $\Delta = 1.5$ mm, thus the circumference of the 5-voxel hole is 18 mm, compared with the real hole circumference of 15.7 mm. The difference in volume is 1.75; thus the absorption of the hole is increased by this factor in our model as compared with the estimated absorption of the experimental liquid.

The experiment was repeated for nine different combinations of the optical properties of the liquid with $\mu_s' = 0.56, 2.3, 9.0\ \mathrm{mm}^{-1}$ and $\mu_a = 0.0018, 0.015, 0.029\ \mathrm{mm}^{-1}$. Figure 8 shows a comparison between the experimental and numerical-model results. The figure shows the ON–OFF contrast, i.e., the ratio of light detected during the first 230 ps when the measurement is performed through the sample in the region of the hole, divided by the amount of light detected in the same time window when the measurement is performed through the sample perpendicular to the surface, 15 mm from the vertical plane containing the cylindrical hole [Fig. 8(a)]. Thus, a value larger than 1 represents more early light in the hole region, and a value less than 1 represents less early light detected from that region. The symbols represent the experimental data, with error bars.

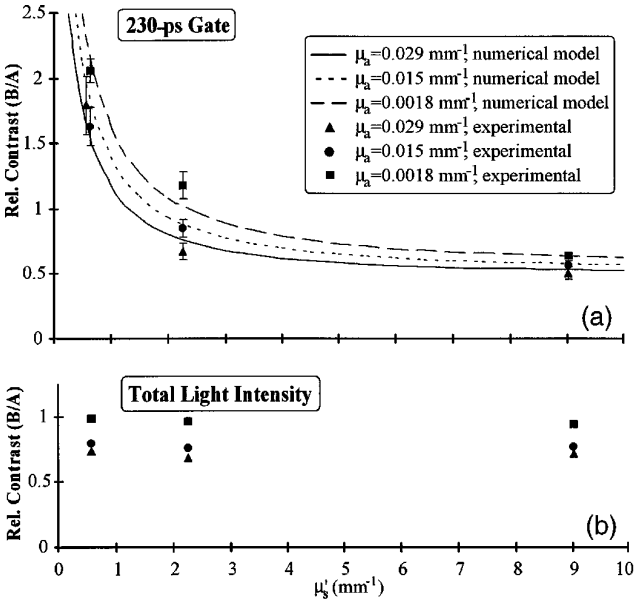

Fig. 8. Relative contrast B/A, i.e., the amount of light in a 230-ps time-gate window for a measurement over the hole, B, divided by the amount of light detected in the same time window for a measurement 15 mm beside the hole, A, as a function of the effective scattering coefficient μ_s' of the liquid in the hole: (a) The symbols represent the experimental data, and the curves represent the numerical-model data for different values of the absorption coefficient μ_a of the liquid in the hole. (b) The experimental ratio in the total light intensity for the two measuring sites.

Three different sets of data represent the different absorption coefficients of the liquid in the hole. Data are shown for various scattering coefficients of the liquid in the hole as well. The results show a good agreement between the experimental data and the data obtained with the numerical model. There is some difference at low scattering, but in this region the gradient of the curve is steep, making it sensitive to small variations in the scattering coefficient. Figure 8(b) shows the ratio B/A in the total light intensity for the experimental data.

A set of simulations were performed with the optical properties of the bulk material being closer to those of real tissue ($\mu_s' = 1.1\ \text{mm}^{-1}$ and $\mu_a = 0.05\ \text{mm}^{-1}$). The optical properties of the 5-voxel cross-approximated cylinder were altered between values of $\mu_s' = 0.2$–$2.2\ \text{mm}^{-1}$ and $\mu_a = 0.005$–$0.1\ \text{mm}^{-1}$. Figure 9 shows a calculated surface plot representing the same ON–OFF contrast that was described for Fig. 8. The axes at the bottom represent the different absorption and scattering coefficients of the hidden cross-approximated cylinder. It should be noted that, in the region where scattering is low and absorption is high, the diffusion approximation is probably not valid because scattering is only of the order of 2–3 times larger than absorption.

4. Discussion

Optical techniques for tissue diagnostics provide some characteristics that make them potential candidates for future clinical use. Light diagnostics is nonintrusive, and the radiation in the visible and near-infrared regions is not harmful. As for all new modalities, it is most interesting to evaluate such techniques in cases for which the existing techniques are not so well suited. For the purpose of breast-tumor detection, conventional x-ray mammography detects most tumors well. This technique has, however, some less attractive features.

The ionizing radiation used is connected with some small risk for patients in terms of mutagenicity. This risk is of special interest to the discussion of screening large populations for breast tumors. It would therefore be of great advantage if one could find an alternative method that diagnoses breast tumors with the same accuracy but without this risk. There is also an interest in developing new diagnostic techniques to be used as a complement to conventional x-ray mammography, as this technique, after all, is not able to identify all tumors. It has been shown that it is difficult to detect some tumor types, e.g., comedo structures, with conventional mammography, especially in the dense breast tissue of young women.[31] Optical transillumination imaging might be a technique that could be developed to serve any of these purposes.

Time-resolved detection in optical transillumination imaging is used for two purposes: it permits imaging with an improved spatial resolution and also makes it possible to utilize the scattering properties of the tissue in the diagnostics, so that one is not limited to differences in the absorption coefficient only.

Our experiments show that the influence of scattering is very high during time-gated viewing. Figure 4 shows that an object with a scattering coefficient different from the surrounding medium could be detected by the use of time-resolved detection tech-

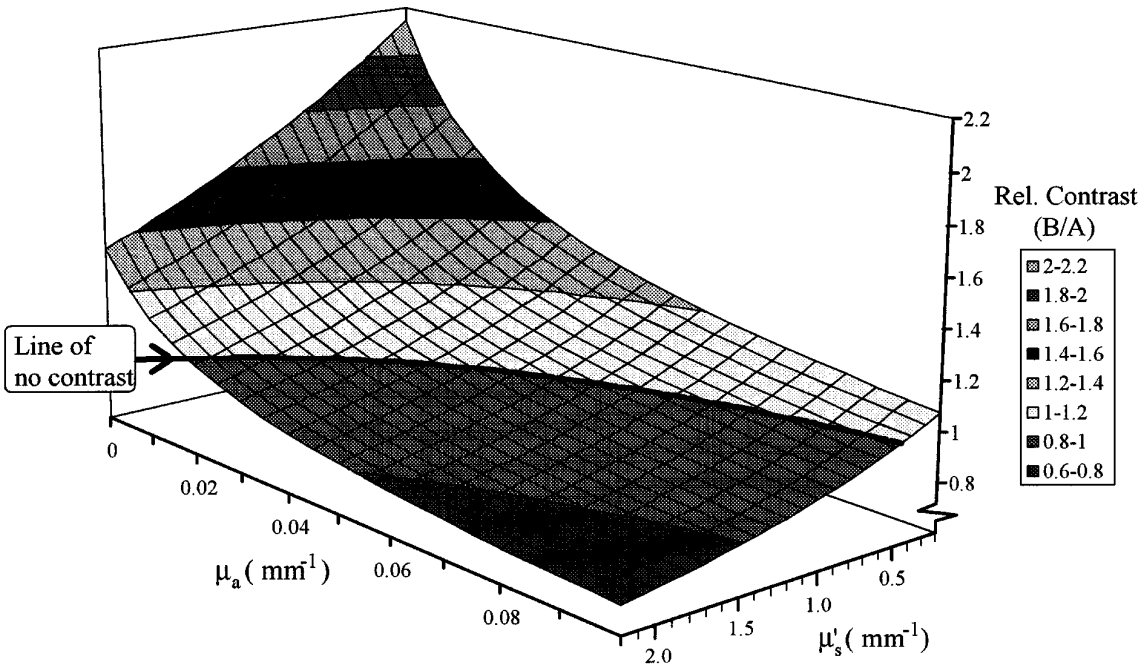

Fig. 9. Surface plot representing the same ON–OFF contrast that was described for Fig. 8(a). The axes at the bottom represent the different absorption and scattering coefficients of the hidden, cross-approximated cylinder. The optical properties of the bulk material were $\mu_s' = 1.1\ \text{mm}^{-1}$ and $\mu_a = 0.05\ \text{mm}^{-1}$.

niques. This would not be possible in the steady-state case. Furthermore, in the geometry used here an increased spatial resolution can be achieved as a result of the suppression of multiple-scattered light. Our experiment shows that it is possible to detect subcentimeter features, with scattering properties that differ from their surroundings, inside a highly scattering phantom with a thickness realistic for mammography. This result is in agreement with those reported by others.[32] The phantom we used is a worst-case condition for transillumination: the scattering is higher and the absorption lower than for breast tissue. Figure 5 shows that the relative contrast of a hole in the center of the phantom was dependent on the hole size. A hole less than approximately 4 mm could not be detected. The FWHM of the detected peak was rather constant for the different hole diameters. We believe that this consistency reflects the highest spatial resolution detectable in this time window with the use of a phantom that has the high scattering coefficient of Delrin. We also show that the location of the lesion inside the volume is of great importance to the possibility of its detection (see Fig. 6). The closer the lesion is to one of the borders, the easier it is to detect. This relation is also found in traditional diaphanography.

It is shown that our computer model works well to solve the diffusion equation numerically, making it possible to study the influence of inhomogenities in tissue (Figs. 7 and 8). In Fig. 8(b) it can be seen that the total light intensity is insensitive to variations in the scattering coefficient. On the other hand, the sensitivity to variations in the absorption coefficient seems to be approximately the same for the gated and the total light. Figure 9 shows the possibility of detection of a hidden lesion, depending on the differences in the optical properties between the bulk tissue and the lesion. Note that there is a line in Fig. 9 across the surface, representing a value of 1, where there is no contrast between the lesion region and the region located 15 mm from the lesion. Thus, the use of the time-gated technique gives rise to some critical combinations of the scattering and absorption coefficients of the lesion when it cannot be detected. This limitation could be circumvented by the use of a more sophisticated evaluation procedure, for instance, using several time gates or using the whole time-dispersion curve for data evaluation.

Even though we use a time gate that is rather long compared with other time-gating techniques, we show that we can increase the spatial resolution, as compared with cw techniques, and detect objects with a wide range of scattering properties. Because of this long time gate, which means that a relatively big fraction of the total light is used in detection (in this case approximately 0.1%), the total acquisition time for each sample position could be short. To improve the technique and to be able to further shorten the acquisition time, it would be desirable for an evaluation procedure to make use of the whole time-dispersion curve.

A method to reduce the influence of scattering in tissue would be to use longer wavelengths, i.e., 1000–1300 nm, for which tissue scattering is lower but for which water absorption has not yet become significant.[33] In this wavelength region differences in optical properties between malignant and normal tissues have, to our knowledge, not yet been investigated. Absorption will be much more important in this region than for shorter wavelengths, making it easier to obtain a good spatial resolution. But, if the scattering properties constitute the diagnostic criteria for detecting tumors, it is probably better to work at shorter wavelengths.

A general condition for the success of the optical techniques is, of course, that there are differences in the optical properties between healthy and malignant tissues. Some studies have been performed, but they are normally performed *in vitro*.[34] Further studies on tissue optical parameters are required to permit speculation in more detail of the future use of the optical techniques described here.

This research was supported by the Swedish Research Council for Engineering Sciences (TFR), the Swedish Medical Research Council (MFR), and the Swedish Natural Science Research Council (NFR).

References

1. G. J. Müller, B. Chance, R. R. Alfano, S. R. Arridge, J. Beuthan, E. Gratton, M. Kaschke, B. R. Masters, S. Svanberg, and P. van der Zee, eds., *Medical Optical Tomography: Functional Imaging and Monitoring,* SPIE Institute Series Vol. SI11 (Society of Photo-Optical and Instrumentation Engineers, Bellingham, Wash., 1993).
2. R. J. Bartrum and H. C. Crow, "Transillumination lightscanning to diagnose breast cancer: a feasibility study," Am. J. Radiol. **142,** 409–414 (1984).
3. M. Swift, D. Morrell, R. B. Massey, and C. L. Chase, "Incidence of cancer in 161 families affected by ataxia-telangiectasia," N. Engl. J. Med. **325,** 1831–1836 (1991).
4. B. C. Wilson, M. S. Patterson, S. T. Flock, and D. R. Wyman, "Tissue optical properties in relation to light propagation models and in vivo dosimetry," in *Photon Migration in Tissue,* B. Chance, ed. (Plenum, New York, 1989), pp. 24–42.
5. S. Andersson-Engels, R. Berg, S. Svanberg, and O. Jarlman, "Time-resolved transillumination for medical diagnostics," Opt. Lett. **15,** 1179–1181 (1990).
6. B. Chance and A. Katzir, eds., *Time-Resolved Spectroscopy and Imaging of Tissue,* SPIE **1431,** 1–332 (1991).
7. K. G. Spears, J. Serafin, N. H. Abramson, X. Zhu, and H. Bjelkhagen, "Chrono-coherent imaging for medicine," IEEE Trans. Biomed. Eng. **36,** 1210–1221 (1989).
8. H. Chen, Y. Chen, D. Dilworth, E. Leith, J. Lopez, and J. Valdmanis, "Two-dimensional imaging through diffusing media using 150-fs gated electronic holography techniques," Opt. Lett. **16,** 487–489 (1991).
9. M. Toida, T. Ichimura, and H. Inaba, "The first demonstration of laser computed tomography achieved by coherent detection imaging method for biomedical applications," Inst. Electron. Inf. Commun. Jpn. Trans. **E74,** 1692–1694 (1991).
10. K. M. Yoo, Q. Xing, and R. R. Alfano, "Imaging objects hidden in highly scattering media using femtosecond second-harmonic-generation cross-correlation time gating," Opt. Lett. **16,** 1019–1021 (1991).
11. L. M. Wang, P. P. Ho, and R. R. Alfano, "Double-stage

picosecond Kerr gate for ballistic time-gated optical imaging in turbid media," Appl. Opt. **32,** 535–540 (1993).
12. M. D. Duncan, R. Mahon, L. L. Tankersley, and R. Reintjes, "Time-gated imaging through scattering media using stimulated Raman amplification," Opt. Lett. **16,** 1868–1870 (1991).
13. G. W. Faris and M. Banks, "Upconverting time gate for imaging through highly scattering media," Opt. Lett. **19,** 1813–1815 (1994).
14. J. C. Hebden and K. S. Wong, "Time-resolved optical tomography," Appl. Opt. **32,** 372–380 (1993).
15. S. Andersson-Engels, R. Berg, A. Persson, and S. Svanberg, "Multispectral tissue characterization with time-resolved detection of diffusely scattered white light," Opt. Lett. **18,** 1697–1699 (1993).
16. R. Berg, O. Jarlman, and S. Svanberg, "Medical transillumination using short-pulse diode lasers," Appl. Opt. **32,** 574–579 (1993).
17. J. Fishkin, E. Gratton, M. J. vandeVen, and W. W. Mantulin, "Diffusion of intensity modulated near-infrared light in turbid media," in *Time-Resolved Spectroscopy and Imaging of Tissue,* B. Chance and A. Katzir, eds., SPIE **1431,** 122–135 (1991).
18. A. Knüttel, J. M. Schmitt, and J. R. Knutson, "Spatial localization of absorbing bodies by interfering diffusive photon-density waves," Appl. Opt. **32,** 381–389 (1993).
19. S. J. Madsen, E. R. Anderson, R. C. Haskell, and B. J. Tromberg, "Portable, high-bandwidth frequency-domain photon migration instrument for tissue spectroscopy," Opt. Lett. **19,** 1934–1936 (1994).
20. B. Chance, J. S. Leigh, H. Miyake, D. S. Smith, S. Nioka, R. Greenfeld, M. Finander, K. Kaufmann, W. Levy, M. Young, P. Cohen, H. Yoshioka, and R. Boretsky, "Comparison of time-resolved and -unresolved measurement of deoxyhemoglobin in brain," Proc. Natl. Acad. Sci. USA **85,** 4971–4975 (1988).
21. D. T. Delpy, M. Cope, P. van der Zee, S. Arridge, S. Wray, and J. Wyatt, "Estimation of optical pathlength through tissue from direct time of flight measurement," Phys. Med. Biol. **33,** 1433–1442 (1988).
22. R. Berg, S. Andersson-Engels, O. Jarlman, and S. Svanberg, "Time-resolved transillumination for medical diagnostics," in *Time-Resolved Spectroscopy and Imaging of Tissue,* B. Chance and A. Katzir, eds., SPIE **1431,** 110–119 (1991).
23. S. Andersson-Engels, R. Berg, and S. Svanberg, "Effects of optical constants on time-gated transillumination of tissue and tissue-like media," J. Photochem. Photobiol. **16,** 155–167 (1992).
24. M. S. Patterson, B. Chance, and B. C. Wilson, "Time resolved reflectance and transmittance for the noninvasive measurement of optical properties," Appl. Opt. **28,** 2331–2336 (1989).
25. S. L. Jacques, "Time resolved propagation of ultrashort laser pulses within turbid tissue," Appl. Opt. **28,** 2223–2229 (1989).
26. M. S. Patterson, S. J. Madsen, J. D. Moulton, B. C. Wilson, "Diffusion equation representation of photon migration in tissue," MTT-S Digest 905–908 (1991).
27. M. S. Patterson, J. D. Moulton, B. C. Wilson, K. W. Berndt, and J. R. Lakowicz, "Frequency-domain reflectance for the determination of the scattering and absorption properties of tissue," Appl. Opt. **30,** 4474–4476 (1991).
28. W. H. Press, B. P. Flannery, S. A. Teukolsky, and W. T. Vetterling, *Numerical Recipes in Pascal* (Cambridge U. Press, Cambridge, 1990).
29. C. Lindquist, "Numerical diffusion modelling of light propagation in turbid media for medical diagnostics," Lund Rep. At. Phys. **LRAP-157,** 1–47 (1994).
30. J. W. Pickering, S. A. Prahl, N. van Wieringen, J. F. Beek, H. J. C. M. Sterenborg, and M. J. C. van Gemert, "Double-integrating-sphere system for measuring the optical properties of tissue," Appl. Opt. **32,** 399–410 (1993).
31. M. J. Homer, "Breast imaging: pitfalls, controversies and some practical thoughts," Radiol. Clin. North Am. **23,** 459–472 (1985).
32. G. Mitic, J. Kölzer, J. Otto, E. Plies, G. Sölkner, and W. Zinth, "Time-gated transillumination of biological tissues and tissue-like phantoms," Appl. Opt. **33,** 6699–6710 (1994).
33. J. J. Dolne, K. M. Yoo, F. Liu, and R. R. Alfano, "Spatial frequency imaging through random scattering media," in *Advances in Optical Imaging and Photon Migration,* R. R. Alfano, ed., Vol. 21 of OSA Proceedings Series (Optical Society of America, Washington, D. C., 1994), pp. 284–287.
34. V. G. Peters, D. R. Wyman, M. S. Patterson, and G. L. Frank, "Optical properties of normal and diseased human breast tissues in the visible and near infrared," Phys. Med. Biol. **35,** 1317–1334 (1990).

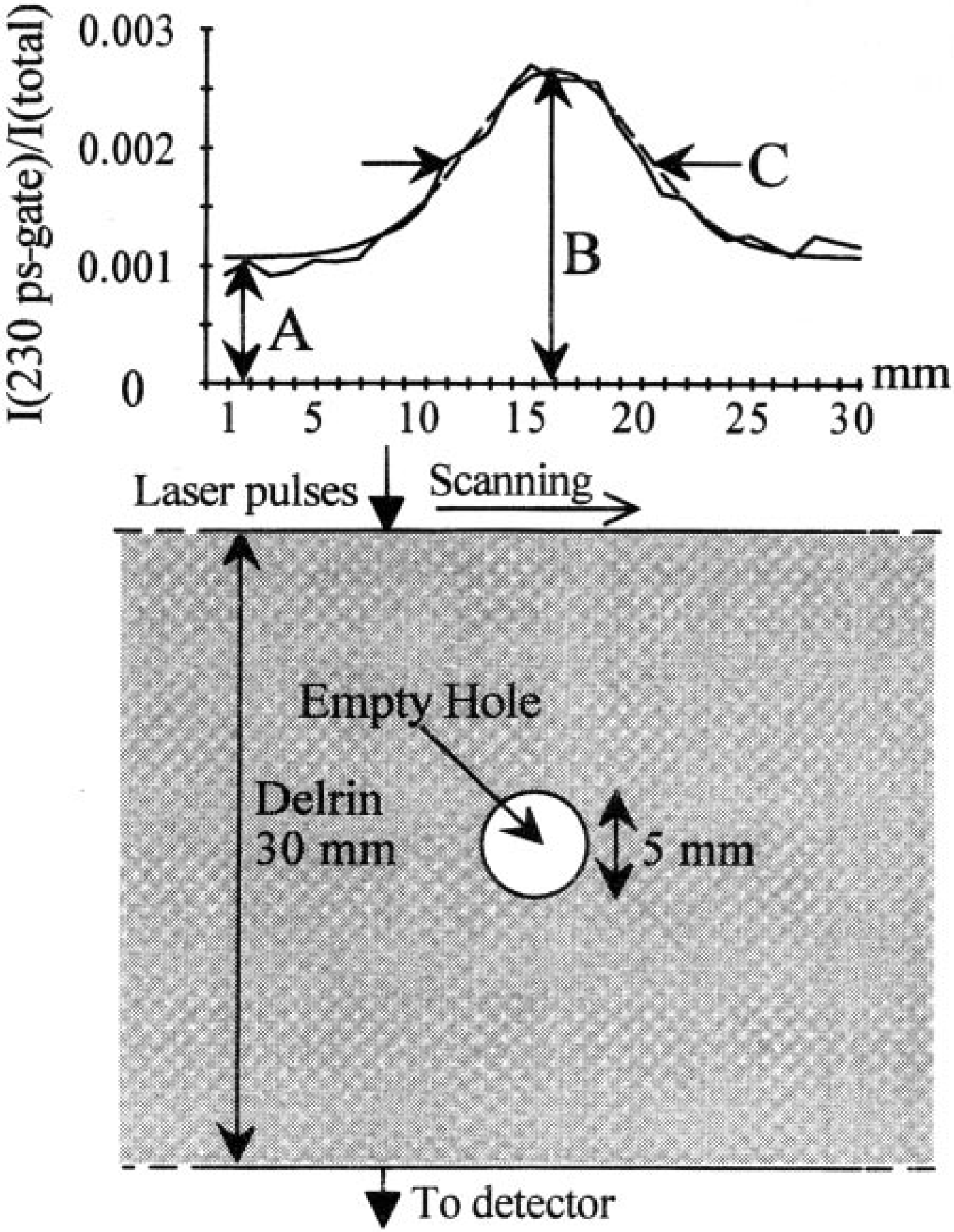
I(230 ps-gate)/I(total)
0.003
0.002
0.001
0
A
B
C
1
5
10
15
20
25
30
mm
Laser pulses
Scanning
Empty Hole
Delrin
30 mm
5 mm
To detector